Cavity-Enhanced Harmonic Generation in Silicon Rich Nitride Photonic Crystal Microresonators

Marco Clementi,[1, a)] Kapil Debnath,[2, 3, b)] Moïse Sotto,[3] Andrea Barone,[1] Ali Z. Khokhar,[4] Thalía Domínguez Bucio,[4] Shinichi Saito,[3] Frederic Y. Gardes,[4] Daniele Bajoni,[5] and Matteo Galli[1]

[1)] *Dipartimento di Fisica, Università degli Studi di Pavia, via Agostino Bassi 6, 27100 Pavia, Italy*

[2)] *Department of Electronics and Electrical Communication Engineering. Indian Institute of Technology Kharagpur, Kharagpur, West Bengal, India-721302*

[3)] *Faculty of Physical Sciences and Engineering, University of Southampton, Southampton SO171BJ UK*

[4)] *Optoelectronics Research Centre, University of Southampton, Southampton SO171BJ UK*

[5)] *Dipartimento di Ingeneria Industriale e dell'Informazione, Università degli Studi di Pavia, via Ferrata 1, 27100 Pavia, Italy*

(Dated: 8 March 2019)

We report second and third harmonic generation in photonic crystal cavities fabricated in a suspended silicon rich nitride (SiN_x) membrane under resonant continuous-wave excitation at telecom wavelength. Two-dimensional photonic crystal cavities with a far-field optimized line-width modulated design were employed. A quality factor at fundamental wavelength as high as $Q = 1.3 \times 10^4$ and a coupling efficiency $\eta_c \approx 30\%$ enabled to exploit the cavity field enhancement to achieve the generation efficiencies $\rho_{SH} = (4.7 \pm 0.2) \times 10^{-7}$ W^{-1} and $\rho_{TH} = (5.9 \pm 0.3) \times 10^{-5}$ W^{-2}. The absence of saturation effects at high power and the transparency of the device at second harmonic wavelength suggest the absence of two-photon absorption and related detrimental effects.

I. INTRODUCTION

One of the most prominent objectives of integrated photonics is the generation and manipulation of light at the nanoscale, with applications ranging from industry to fundamental research, and with important benefits in the emerging field of optical quantum technologies[1–3].

In this framework, photonic crystal (PhC) cavities play a crucial role as building blocks for the manipulation of light on-chip. These structures have the unique capability to localize the optical field with ultra-high quality factor (Q) and diffraction-limited mode volume (V)[4]. Such tight confinement leads to the enhancement of the effective light-matter interaction, which enables to exploit nonlinear and quantum optical effects in an integrated photonic platform with minimum footprint. PhC cavities have indeed demonstrated to be suitable to achieve low-power, on-chip frequency conversion, including four-wave mixing[5] and harmonic generation[6–10] even at continuous wave (CW) regime, nanolasers[11], all-optical switching[12], and strong coupling to single quantum emitters[13].

One of the most employed materials for the fabrication of PhC structures has traditionally been silicon[14], thanks to the large refractive index contrast achievable, which eases the confinement, the high fabrication quality and the compatibility with CMOS fabrication process of the silicon-on-insulator (SOI) platform, which allows to include PhCs in the industrial framework of Silicon Photonics[4,15]. Moreover, despite the centrosymmetric nature of crystalline silicon prohibits an appreciable second-order nonlinear response, this material exhibits a

pronounced third-order nonlinear response, with a nonlinear refractive index of $n_2 = 2.2 \times 10^{-18}$ m^2/W[16], useful for frequency conversion applications. Despite these advantages, the relatively narrow bandgap of silicon presents several issues for nonlinear operation at telecom wavelength. Specifically, two-photon absorption (TPA) processes and related detrimental effects - such as free carrier absorption (FCA) and free carrier dispersion (FCD)[17] - limit the potential performance of these devices, even at coupled powers of few μW[7].

In order to overcome these limitations, several wide-bandgap materials, such as indium phosphide (InP)[18], gallium phosphide (GaP)[6], silicon carbide (SiC)[8] and gallium nitride (GaN)[9,10] have been proposed and tested for frequency conversion applications in PhC cavities. The wide transparency range, combined to a negligible TPA and, in some cases, a strong $\chi^{(2)}$ response of the medium, make these materials good candidates for nonlinear applications in integrated photonic devices.

In the last few years, silicon nitride has gathered increasing attention in the field of Silicon Photonics thanks to the compatibility of its manufacturing process with standard CMOS fabrication, making it a suitable alternative to silicon for nonlinear applications[19,20]. Nonetheless, stoichiometric silicon nitride (Si_3N_4) exhibits a nonlinear response significantly lower than the one of silicon and a relatively low refractive index. A possible pathway to overcome these limitations is to employ specific deposition techniques to increase the relative concentration of silicon[21]. The resulting hybrid material, Silicon Rich Nitride (SRN), provides a Kerr response comparable to the one of silicon, negligible TPA and increased refractive index[16]. Recently, several nonlinear applications of SRN were demonstrated[16,22], as well as its suitability for the fabrication of PhC structures, such as waveguides[23] and

---

[a)]Electronic mail: marco.clementi01@universitadipavia.it

[b)]Electronic mail: k.debnath@ece.iitkgp.ac.in

ultra-high Q PhC cavities[24].

In this letter, we report the low-power generation of second (SH) and third (TH) harmonics in a two-dimensional PhC cavity fabricated in a suspended membrane of SRN under CW resonant excitation at telecom wavelength.

II. DESIGN AND FABRICATION

For the demonstration here detailed, we employed a modified designed originally proposed by Kuramochi *et al.*[25] (also known as A1 cavity) which consists in the adiabatic modulation of the width of a line defect (W1 waveguide), obtained in a hexagonal lattice of holes, as depicted in fig. 1a. The lattice step of the PhC structure was chosen $a = 580$ nm and the hole radius $r = 0.30a$, in order to select a fundamental resonant mode in the telecom wavelength range (C-band, $\lambda_0 \sim 1550$ nm). Optical confinement was achieved by shifting the holes marked in red, yellow and blue by an amount of $\Delta A = 15$ nm, $\Delta B = 10$ nm and $\Delta C = 5$ nm respectively along the y direction.

The normalized efficiency of the n-th order harmonic generation process is expected to scale proportionally to $(\eta_c Q/V)^n$, where $\eta_c = P_{coupled}/P_{incident}$ is the coupling efficiency for resonant excitation from free space, $V = \int \varepsilon \left| E \right|^2 d^3 r / \max\{\varepsilon \left| E \right|^2\}$ is the mode volume and Q is the quality factor of the fundamental mode[7,26]. Thus, our design target was to maximize, for fixed V, the $\eta_c \times Q$ product, rather than the Q factor alone. For this reason, we employed a far-field optimization technique[27] which consists in increasing the radius of specific holes (denoted by bold circles in fig. 1a) in order to engineer the cavity far-field pattern to exhibit a nearly Gaussian profile. The optimization resulted in a significant increase of the η_c related to the transverse mode of the impinging excitation laser, at the cost of a reduced Q factor.

We validated our design via three-dimensional finite-difference time-domain (FDTD) simulations. Employing a mesh cell size of $0.02a_x \times 0.02a_y \times 30$ nm we calculated a Q factor as high as 21,000 for the fundamental mode centered at $\lambda_0 = 1577$ nm and a mode volume $V = 0.73(\lambda/n)^3$. The simulated near- and far-field profiles for the fundamental mode are shown in fig. 1c and 1d.

We fabricated the samples in a 300 nm thick suspended membrane of SRN, obtained by low-temperature Plasma Enhanced Chemical Vapour Deposition (PECVD). For further details about the fabrication process please refer to the work by Debnath *et al.*[24]. Fig. 1b shows a scanning electronic microscope (SEM) image of one of the realized samples.

III. EXPERIMENT AND RESULTS

We performed a linear (low-power) characterization of the fabricated samples by means of the Resonant Scattering (RS) technique[28]. Our experimental apparatus, consisting essentially in a cross-polarized, confocal microscopy setup, is depicted in fig. 2a. We employed a tunable CW laser source (Santec TSL-510, range 1500-1630 nm) for the excitation of the fundamental cavity mode. The collimated laser beam, after passing a thin-film polarizer (TFP), was focused on the sample using a high numerical aperture microscope objective (Nikon 50x, NA=0.8). The optical cavity was placed in the focal plane and rotated at 45° with respect to the impinging polarization. The orthogonal polarization was then collected via the same excitation pathway through a second TFP, coupled to a single-mode optical fiber and finally sent to a InGaAs-based photodetector. By scanning the input wavelength, we were able to measure the spectral response of the cavities.

By employing lithographic tuning of the fabrication parameters (fig. 2c and 2d), we were able to select the sample which maximizes the figure of merit $\eta_c \times Q$. We found the optimal value for a cavity with modification of the holes' radii $\Delta r = +12$ nm, for which we measured a resonance wavelength $\lambda_0 = 1546.3$ nm and a quality factor $Q = 13,000$, as retrieved from Fano fit of the measured RS spectrum[28], represented in fig. 2b. The measured values of coupling efficiency and figure of merit are reported in fig. 2c-d.

In order to evaluate the coupling efficiency, we compared the peak RS signal at the resonance wavelength with the one measured by replacing the sample with a reference mirror and aligning the polarizers in parallel directions[7]. We were thus able to estimate a coupling efficiency from free-space to the cavity as high as $\eta_c \approx 30\%$. We expect this value to be limited mainly by 1) the mode mismatch of the focused Gaussian beam with the far-field pattern and 2) the finite numerical aperture of the optical system.

We then probed the nonlinear response of the selected cavity. We employed the same apparatus to collect the generated SH and TH signal, and included a dichroic mirror (DM) and an appropriate sequence of filters to separate it from the pump at fundamental wavelength. We imaged the near-field of generated harmonics on a silicon-based CCD camera (PI Acton, liquid nitrogen cooled). By increasing the pump power, we were able to observe the generation of light at SH and TH wavelengths (fig. 3), which we later confirmed by spectroscopic measurements (fig. 4a-b).

Fig. 3a shows the generated SH emission from the sample. The large modal area suggests transparency of the SRN material at $\lambda_{SH} = 773.2$ nm. As the material consists in an amorphous deposition[21], we hypothesize that the intrinsic $\chi^{(2)}$ response of the medium is averaged to zero on the ensemble. The physical origin of the observed phenomenon relies then in the breaking of inversion sym-
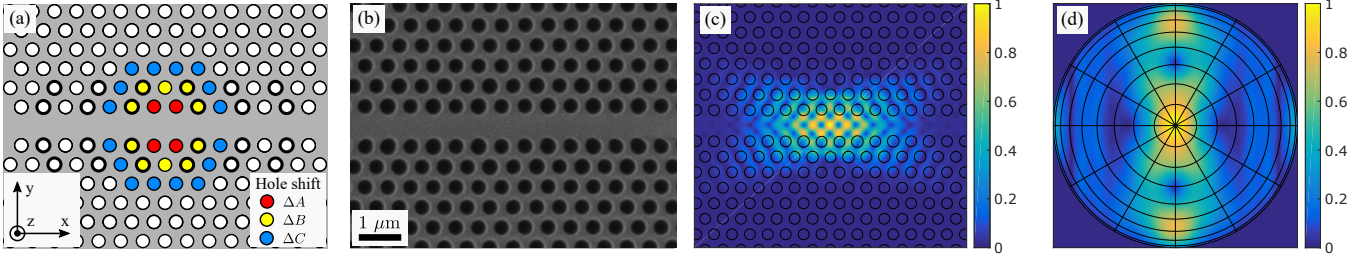
FIG. 1. (a) Schematic of the PhC cavity design. The red, yellow and blue holes are shifted on the y-axis away from the line defect of an amount $\Delta A = 15$ nm, $\Delta B = 10$ nm and $\Delta C = 5$ nm respectively. The holes marked by bold circles are characterized by a radius larger than the nearby holes of $\Delta r = +12$ nm, in view of an optimized coupling to the free-space excitation mode. (b) SEM image of the fabricated sample. Nominal parameters are specified in the main text. (c) Simulated near-field profile of the fundamental resonance mode (in-plane electric field amplitude $|E|$, normalized linear scale). (d) Far-field projection of the simulated fundamental resonant mode (electric field amplitude $|E|$). The main lobe at $\theta = 0$ was optimized to match a focused Gaussian beam profile impinging orthogonal to the cavity plane. Grid ranges from $0°$ to $90°$.
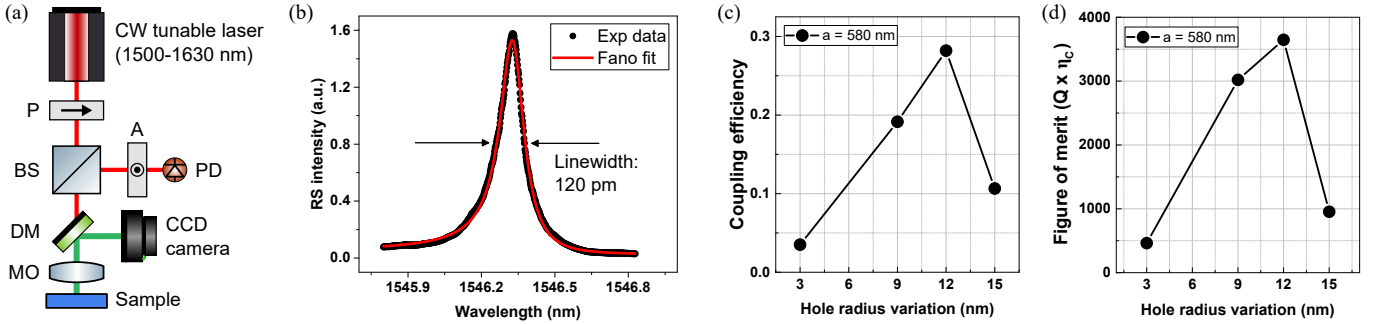

FIG. 2. (a) Schematic of the experimental apparatus. The collimated light from a CW tunable source is polarized (P) and focused through a microscope objective (MO) on the sample, which is placed in the focal plane at $45°$ with respect to the laser polarization. The same excitation path is used to collect the RS signal and the generated SH and TH, which are separated from the pump via a dichroic mirror (DM) and imaged on a CCD camera. The RS signal is then filtered by a crossed polarizer (A) and collected by a InGaAs-based photodetector (PD). (b) RS spectrum and Fano fit for the fundamental (pump) resonant mode of the cavity. (c) Estimated coupling efficiency and (d) figure of merit ($\eta_c \times Q$) for selected samples as a function of the radius variation Δr introduced to optimize the coupling to far-field.

metry mainly provided by the multiple interfaces between the bulk material and the air holes. Since the structure is not resonant at the SH wavelength, the signal here generated couples to the quasi-guided (leaky) modes of the PhC slab and eventually radiates outside the the membrane.

Fig. 3b shows the generated TH. Because of the bulk nature of the nonlinear process, the TH near-field profile mimics the one of the fundamental mode, as one can notice by comparison with fig. 1c. A qualitative comparison between fig. 3a and fig. 3b suggests that the material absorption at $\lambda_{TH} = 515.4$ nm is significant. This datum was confirmed by ellipsometric measurements, which highlighted an absorption band edge wavelength of 600 nm. The underlying physical mechanism here is the following: the TH is originated from the bulk $\chi^{(3)}$ nonlinearity of the material, which is expected to be larger than the one of stoichiometric silicon nitride[16], but it is soon absorbed by the material itself. The small fraction of TH light which is not absorbed can be then observed in the experiment, and closely follows

the near field profile of the fundamental (localized) mode.

Fig. 4b illustrates the spectral response of the system for large coupled power. The relatively large coupled power ($P_{coupled} \approx 1$ mW) induces heating of the cavity region, originated by the linear absorption of the material[24] at resonance wavelength. Thus, the measured spectrum exhibits a markedly asymmetric, sawtooth-shaped response, which is a characteristic signature of the regime of optical bistability[29–31], in this case originated by thermo-optic effect due to residual linear absorption of the silicon-rich nitride material. The plotted SH and TH spectra are acquired simultaneously with the fundamental (pump) RS spectrum and clearly follow the squared and cubed trend of the latter respectively, confirming the cavity-enhanced nature of the nonlinear processes under investigation.

In order to confirm the validity of our observations, we characterized the power scaling trend of the nonlinear processes. The analysis is represented in fig. 4c. By varying the input power to our setup and tuning the wavelength of the excitation laser to compensate for the
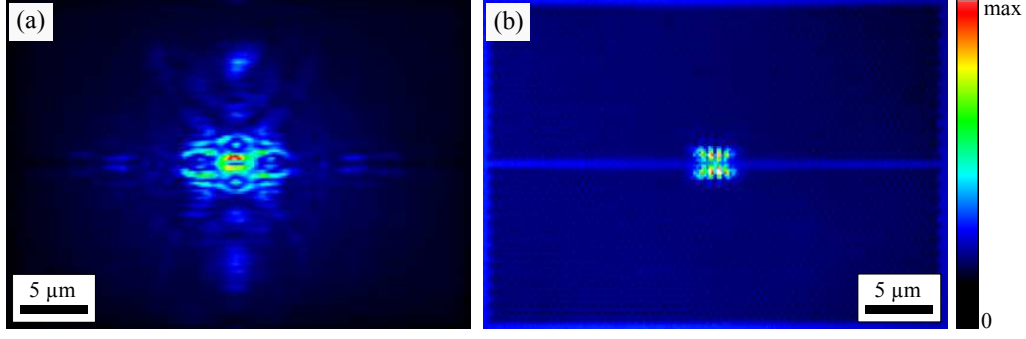
FIG. 3. False color images of the generated (a) SH and (b) TH near-field profiles (linear scale). The sample background was artificially illuminated for sake of clarity.
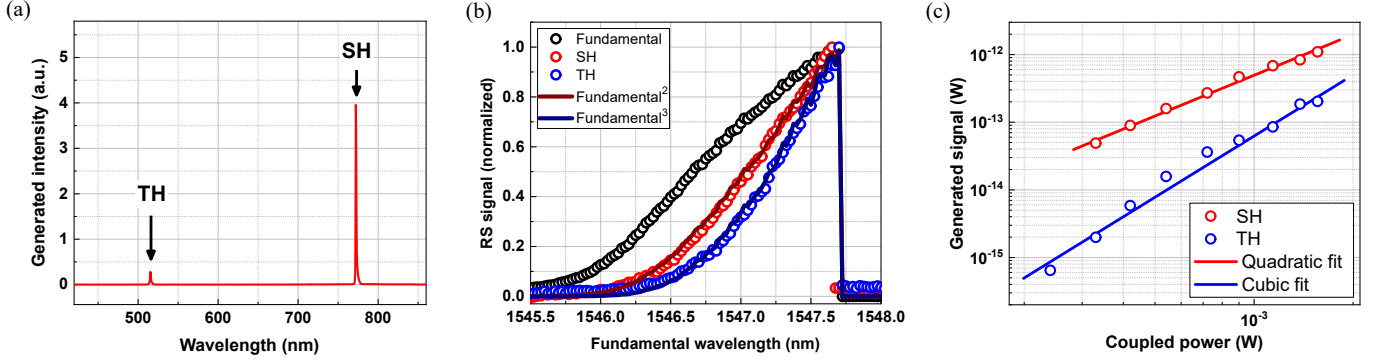

FIG. 4. (a) Sample spectrum of the resonantly generated SH and TH. (b) High power spectrum of the cavity resonance and comparison with the generated SH and TH signals. The large coupled power ($P_{coupled} \approx 1$ mW) leads the system to operate at a regime of strong thermo-optic bistability[29–31], providing the characteristic sawtooth-shape to the spectrum at fundamental wavelength. The generated SH and TH signals closely follow the squared and cubed trend of the fundamental RS signal respectively, highlighting the cavity-enhanced, nonlinear nature of the phenomenon under investigation. (c) Scaling trends of the (peak) generated SH and TH signals. The pump wavelength was systematically adjusted in order to compensate for thermo-optic shift of the resonance. Experimental deviations from the expected trends are mainly related to 1) strong background for points at low power and 2) thermo-optic instability[24,29] for points at high power.

thermo-optic shift of the resonance[24,29], we were able to scan the coupled power at the fundamental wavelength from few μW to 1.6 mW. We estimated the total collected power by integrating over the region-of-interest of our CCD detector. The plot shows with good confidence a quadratic and cubic scaling trend for the generated SH and TH respectively. From the best fit of our results we were able to estimate the normalized generation efficiencies $\rho_{SH} = P_{SH}/P_{coupled}^2 = (4.7 \pm 0.2) \times 10^{-7}$ W^{-1} and $\rho_{TH} = P_{TH}/P_{coupled}^3 = (5.9 \pm 0.3) \times 10^{-5}$ W^{-2}. It should be remarked that these results represent extrinsic values, as they do not take in to account the fraction of generated power which is not collected by the optical system as it is absorbed, coupled to the guided mode of the membrane or scattered outside the numerical aperture of the system. However, these values provide a lower bound on the effective efficiency of the process for practical applications and we believe that they can be significantly improved by engineering the extraction mechanism of the generated signal from the cavity at the SH and TH frequencies.

To provide a term of comparison, generation efficiencies of the order of $\rho_{SH} \approx 10^{-5}$ W^{-1} and $\rho_{TH} \approx 10$ W^{-2} were reported in silicon-based PhC cavities[7], while the relevant data for microring resonators based on stoichiometric silicon nitride[32] are $\rho_{SH} \approx 10^{-3}$ W^{-1} and $\rho_{TH} \approx 10^{-9}$ W^{-2}. It should be remarked that the former platform exhibits a tighter confinement than the one here presented, due to the higher refractive index contrast of the silicon/air interface, while the latter is characterized by a weaker confinement due to the lower refractive index and the significantly larger mode volume. It should be also noted that the SH generation efficiency reported here is significantly lower compared to materials exhibiting non-vanishing bulk second order nonlinearity[6,8,10,31], with measured values of generation efficiency ranging from $\rho_{SH} \approx 2 \times 10^{-3}$ W^{-1} to $\rho_{SH} \approx 4$ W^{-1}. We remark that a quantitative comparison between harmonic generation efficiencies in different resonant photonic devices would require the knowledge of the second and third-order nonlinear polarization in the presence of highly anisotropic nanostructured surfaces,

as in the case of photonic crystal nanocavities. This non trivial task is, however, beyond the scope of the present work.

Remarkably, the data presented here highlight the absence of saturation effects due to TPA[17], typical of silicon-based devices. A quantitative comparison may be obtained by looking at the power-dependent generation efficiency curves reported by Galli *et al.*[7] for silicon PhC cavities having a figure of merit $\eta_c \times Q = 4000$ and a Q factor and mode volume very similar to those presented in this work. Indeed, while silicon cavities display a clear saturation of the SHG and THG signals for coupled power of a few tens of μW, our SRN cavities do not show any evidence of saturation even for coupled powers in the mW range. This result confirms the suitability of SRN as a valid alternative to silicon for the fabrication of CMOS compatible integrated nonlinear optical devices.

IV. CONCLUSIONS

In this work, we demonstrated the generation of SH and TH in SRN PhC cavities, from a fundamental resonant CW pump at telecom wavelength. By combining an optimized design for nonlinear operation with an established fabrication process, we demonstrated harmonic generation for up to few mW of coupled pump powers, without incurring in saturation effects related to TPA. Our results suggest the suitability of SRN as a CMOS compatible material platform for integrated low-power nonlinear optical applications.

ACKNOWLEDGMENTS

REFERENCES

[1]W. Bogaerts, P. De Heyn, T. Van Vaerenbergh, K. De Vos, S. Kumar Selvaraja, T. Claes, P. Dumon, P. Bienstman, D. Van Thourhout, and R. Baets, Laser & Photonics Reviews 6, 47 (2012), arXiv:arXiv:1208.0765v1.

[2]D. Thomson, A. Zilkie, J. E. Bowers, T. Komljenovic, G. T. Reed, L. Vivien, D. Marris-Morini, E. Cassan, L. Virot, J.-M. Fédéli, J.-M. Hartmann, J. H. Schmid, D.-X. Xu, F. Boeuf, P. O'Brien, G. Z. Mashanovich, and M. Nedeljkovic, Journal of Optics 18, 073003 (2016).

[3]I. a. Walmsley, Science 348, 525 (2015).

[4]M. Notomi, Reports on Progress in Physics 73, 096501 (2010).

[5]S. Azzini, D. Grassani, M. Galli, D. Gerace, M. Patrini, M. Liscidini, P. Velha, and D. Bajoni, Applied Physics Letters 103 (2013), 10.1063/1.4812640, arXiv:arXiv:1307.5206v1.

[6]K. Rivoire, Z. Lin, F. Hatami, W. T. Masselink, and J. Vučković, Optics Express 17, 22609 (2009), arXiv:0910.4757.

[7]M. Galli, D. Gerace, K. Welna, T. F. Krauss, L. O'Faolain, G. Guizzetti, L. C. Andreani, L. O. Faolain, G. Guizzetti, and L. C. Andreani, Optics Express 18, 26613 (2010).

[8]S. Yamada, B.-S. Song, S. Jeon, J. Upham, Y. Tanaka, T. Asano, and S. Noda, Optics Letters 39, 1768 (2014).

[9]Y. Zeng, I. Roland, X. Checoury, Z. Han, M. El Kurdi, S. Sauvage, B. Gayral, C. Brimont, T. Guillet, M. Mexis, F. Semond, and P. Boucaud, Applied Physics Letters 106 (2015), 10.1063/1.4913679.

[10]M. S. Mohamed, A. Simbula, J.-F. Carlin, M. Minkov, D. Gerace, V. Savona, N. Grandjean, M. Galli, and R. Houdré, APL Photonics 2, 031301 (2017), arXiv:1609.07917.

[11]K. Nozaki, S. Kita, and T. Baba, Optics Express 15, 7506 (2007).

[12]K. Nozaki, T. Tanabe, A. Shinya, S. Matsuo, T. Sato, H. Taniyama, and M. Notomi, Nature Photonics 4, 477 (2010).

[13]K. Hennessy, A. Badolato, M. Winger, D. Gerace, M. Atatüre, S. Gulde, S. Fält, E. L. Hu, and A. Imamoğlu, Nature 445, 896 (2007), arXiv:0610034 [quant-ph].

[14]A. Birner, R. B. Wehrspohn, U. M. Gösele, and K. Busch, Advanced Materials 13, 377 (2001).

[15]M. Settle, M. Salib, A. Michaeli, and T. F. Krauss, Optics Express 14, 2440 (2006).

[16]C. Lacava, S. Stankovic, A. Z. Khokhar, T. D. Bucio, F. Y. Gardes, G. T. Reed, D. J. Richardson, and P. Petropoulos, Scientific Reports 7, 22 (2017).

[17]P. E. Barclay, K. Srinivasan, and O. Painter, Optics Express 13, 801 (2005).

[18]M. W. McCutcheon, J. F. Young, G. W. Rieger, D. Dalacu, S. Frédérick, P. J. Poole, and R. L. Williams, Physical Review B 76, 245104 (2007).

[19]D. J. Moss, R. Morandotti, A. L. Gaeta, and M. Lipson, Nature Photonics 7, 597 (2013).

[20]A. Billat, D. Grassani, M. H. P. Pfeiffer, S. Kharitonov, T. J. Kippenberg, and C.-S. Brès, Nature Communications 8, 1016 (2017), arXiv:1701.03005.

[21]T. Domínguez Bucio, A. Z. Khokhar, C. Lacava, S. Stankovic, G. Z. Mashanovich, P. Petropoulos, and F. Y. Gardes, Journal of Physics D: Applied Physics 50, 025106 (2017).

[22]C. Lacava, S. May, D. Richardson, G. Reed, M. Sorel, and P. Petropoulos, in Conference on Lasers and Electro-Optics, c (OSA, Washington, D.C., 2018) p. JTu2A.64.

[23]K. Debnath, T. D. Bucio, A. Al-Attili, A. Z. Khokhar, S. Saito, and F. Y. Gardes, Optics Express 25, 3214 (2017).

[24]K. Debnath, M. Clementi, T. D. Bucio, A. Z. Khokhar, M. Sotto, K. M. Grabska, D. Bajoni, M. Galli, S. Saito, and F. Y. Gardes, Optics Express 25, 27334 (2017).

[25]E. Kuramochi, M. Notomi, S. Mitsugi, A. Shinya, T. Tanabe, and T. Watanabe, Applied Physics Letters 88, 041112 (2006).

[26]M. W. McCutcheon, D. E. Chang, Y. Zhang, M. D. Lukin, and M. Loncar, Optics Express 17, 22689 (2009), arXiv:0903.4706.

[27]S. L. Portalupi, M. Galli, C. Reardon, T. Krauss, L. O'Faolain, L. C. Andreani, and D. Gerace, Optics Express 18, 16064 (2010).

[28]M. Galli, S. L. Portalupi, M. Belotti, L. C. Andreani, L. O'Faolain, and T. F. Krauss, Applied Physics Letters 94, 1 (2009).

[29]T. Carmon, L. Yang, and K. J. Vahala, Optics Express 12, 4742 (2004).

[30]L.-D. Haret, T. Tanabe, E. Kuramochi, and M. Notomi, Optics Express 17, 21108 (2009).

[31]S. Buckley, M. Radulaski, K. Biermann, and J. Vučković, Applied Physics Letters 103, 211117 (2013), arXiv:1308.6051.

[32]J. S. Levy, M. A. Foster, A. L. Gaeta, and M. Lipson, Optics Express 19, 11415 (2011), arXiv:arXiv:1010.6042v1.